



Small-scale measurement of the transition in fracture behavior of marine sediments

Kelly M. Dorgan^{1,2} · Grant Lockridge^{1,3} · William Cyrus Clemo^{1,2}

Received: 24 March 2023 / Accepted: 2 November 2023 / Published online: 16 December 2023
© The Author(s) 2023

Abstract

Bubbles grow and burrows extend through cohesive, muddy marine sediments by fracture. In contrast, sands are non-cohesive, granular materials. Natural sediments comprised of heterogeneous mixtures of muds and sands are common in coastal areas and provide important habitat for infaunal animals. To explore the transition from cohesive to non-cohesive mechanical behavior of natural sediments, we modified a probe designed for measuring fracture toughness (K_{Ic}). The helical probe is rotated and translated into sediment to grip a plug of sediment, then translated upward to break off the plug while force is measured. Fracture toughness is calculated from the peak net force. The probe shows clearly distinct results in muddier sediments, in which fracture occurs, and in sandier sediments, in which no fracture occurs. The modified probe is limited to near-surface sediments, but it provides a novel method for distinguishing cohesive sediments with tensile strength from non-cohesive sediments on scales relevant for burrowing animals or bubble growth. This measurement allows for comparison of surface and subsurface cohesion and for assessing how tensile strength depends on other properties of sediments.

Keywords Burrowing · Geotechnical properties · Linear elastic fracture mechanics · Muddy sediment

1 Introduction

Bubbles grow and worms burrow through cohesive muddy marine sediments by fracture [12, 18]. Burrowing animals apply forces to burrow walls that are amplified at the tip of the crack-shaped burrow; once enough tensile stress is amplified at the crack tip, the burrow extends anteriorly by fracture [10]. Fracture of muds by bubbles and burrowing animals follows linear elastic fracture mechanics, suggesting that these soft, near-surface muds behave elastically under these small tensile stresses [10, 18]. In contrast, sands are granular materials that lack cohesion and whose responses to forces are governed by the gravitational forces acting on individual grains [23]. Bubbles that grow by fracture in muds are disk shaped, whereas bubbles in sands

are spherical, reflecting the different mechanical responses of muds and sands to small stresses [5]. Similarly, burrows are extended by fracture in muds and by grain rearrangement, excavation, or fluidization in sands [9].

Natural sediments, however, often comprise heterogeneous mixtures of mud- and sand-sized grains, especially in coastal areas where physical and biological processes deposit, resuspend, and mix sediments. Heterogeneous coastal sediments provide important habitat for infaunal organisms whose burrowing and irrigation activities both modify and depend on sediment properties [21, 22, 24, 26]. Whether sediments behave cohesively or non-cohesively is potentially important in characterizing habitat suitability and the behaviors of infauna [11], and the impacts of those behaviors on geotechnical and geochemical processes in sediments [30]. Where the transition from cohesive muds that fail under tension by fracture to non-cohesive, granular responses of sandy sediments falls along this continuum of grain size mixtures is not well understood. Volkenborn et al. [30] found that bioirrigation by lugworms in low-permeability, muddy sands resulted in localized plumes of porewater ascending from the sediment, likely through fractures, whereas coarser, more permeable sediments had

✉ Kelly M. Dorgan
kdorgan@disl.org

¹ Dauphin Island Sea Lab, Dauphin Island, AL 36528, USA

² School of Marine and Environmental Sciences, University of South Alabama, Mobile, AL 36608, USA

³ Present Address: Naval Research Laboratory, Stennis Space Station, MS 39529, USA

more even porewater flow [30]. Sediments also vary in bulk density (or in porosity) and in the quantity and composition of the organic material coating the grains [20]. Extracellular polymeric substances (EPS), comprised of carbohydrates and proteins, have been shown to increase adhesion and cohesion and therefore resistance to erosion of surface sediments [6, 8, 15]. In this context, “cohesion” refers to attraction between similar components of the sediment, and “adhesion” refers to attraction between dissimilar particles, e.g., polymeric substances and mineral grains [15, 19]. Sediment compaction and the cohesion and adhesion of the organic matter may also impact the transition from fracture of cohesive sediments to non-cohesive behavior in subsurface sediments.

Fracture toughness (K_{Ic}) is a material property that describes the resistance of the material to fracture—tougher materials (with higher K_{Ic}) require more force to crack [1]. In soils, fracture occurs when the stress at the crack tip exceeds the tensile strength [23]. If the mechanism by which sediments fail or grains are separated from each other under tension is by fracture, then sediments with high fracture toughness also have high tensile strength. Saturated clean sands are granular materials that lack cohesion, and therefore, fracture toughness is not a relevant parameter in these materials [5]. Thus, the limit at which fracture toughness goes to zero can be considered the effective transition from the cohesive behavior of muds (resulting in bulk tensile strength) to non-cohesive behavior of granular sands. This transition is clearly not discrete in natural, heterogeneous sediments.

Sediment stiffness (E) is also an important material property in burrow extension—if the sediment is stiffer, it resists deformation, allowing worms to apply larger forces to their burrow walls [11]. Burrowing animals act like wedges that push apart the crack walls a distance limited to half the body thickness on each side [10]. The stiffness determines how much force is applied through displacement of the material by that wedge, and the fracture toughness determines whether the crack extends under that force. This ratio of fracture toughness to stiffness affects burrowing behaviors in ways consistent with fracture theory. Burrowers in transparent sediment analogs with high fracture toughness relative to stiffness (K_{Ic}/E) exhibit behaviors consistent with extending a burrow through a tough material by fracture—they expand the thickness of their bodies, especially near the crack tip [11]. In contrast, burrowers in sediment analogs with low fracture toughness relative to stiffness exhibit behaviors consistent with resisting being compressed by a stiff material—they extend the crack-shaped burrow both laterally and anteriorly to reduce the elastic restoring force compressing their bodies [11]. The shape of bubbles that grow by fracture in elastic materials such as sediments similarly depends on these

material properties: Bubbles in materials that fracture easily, i.e., have low fracture toughness relative to stiffness (K_{Ic}/E), are flat and disk-shaped, whereas bubbles in materials with higher K_{Ic}/E are thicker and more spherical [18]. These differences in shape correspond to different ratios of surface area to volume and therefore affect the growth rates of bubbles by diffusion of gases, e.g., of methane in sediments [14].

Although fracture toughness and stiffness are important material properties of muddy sediments, very few measurements of fracture toughness or stiffness on the scales of burrowers or bubbles (i.e., millimeters) have been conducted in natural sediments [3, 5, 17, 18]. Additionally, the limits of elastic behavior on these scales in muddy sediments in terms of grain size, porosity, or other geological parameters are not well understood. Fracture toughness has been measured in sediments by injecting a bubble through the bottom of a mud core, measuring the pressure to grow the bubble, and relating the pressure and volume to fracture toughness using linear elastic fracture mechanics theory [18]. An in situ probe to measure fracture toughness more easily and with much greater spatial resolution was later developed [17]. The probe was tested in intertidal muddy sediments and showed increasing fracture toughness with depth in sediments, as well as horizontal spatial variability across the tidal flat, with higher toughness in the channel than in the flats [3]. The aim of this study was to assess and modify the fracture toughness probe developed by [17] to distinguish between cohesive sediments, in which fracture toughness (K_{Ic}) is defined and > 0 , and non-cohesive, granular sediments.

2 Materials and procedures

2.1 Background theory and previous measurements of fracture toughness

Fracture toughness in linear elastic materials can be quantified in two distinct ways: as the stress amplification needed at the crack tip to result in fracture (the critical stress intensity factor, K_{Ic} , $\text{Pa m}^{0.5}$) or as the stored energy released when fracture occurs (the energy release rate, G_c , J m^{-2}) [1]. The critical stress intensity factor can be measured experimentally, using analytical solutions for stress intensity factor (K_I), which have been derived for many different geometries [27]. For example, Johnson et al. measured K_{Ic} in sediments by injecting a bubble into mud and measuring the internal pressure of the bubble as air was added to expand the bubble [18]. Growth by fracture resulted in a sawtooth pattern of pressure, with pressure increasing as air was injected until the crack extended, causing pressure to decrease rapidly [18]. The equation for

growth of a penny-shaped crack was used to convert the peaks in pressure when fracture occurred to K_{Ic} [18]. Here, “ c ” refers to the critical value of K_I , and “ I ” refers to mode I fracture: Both burrowers and bubbles apply stress to the crack walls perpendicular to the direction of crack growth, which is amplified at the crack tip resulting in high tensile stress; crack propagation occurs through what is known as Mode I fracture (in other modes, fracture occurs through shear) [1, 13, 18].

The laboratory measurements of K_{Ic} on sediment cores done by Johnson et al. [18] by injecting bubbles in sediments and measuring the pressure as bubbles grew provided the first data on fracture toughness in natural sediments, but the method was time-consuming and not easily transferrable to the field. Johnson et al. [17] therefore developed an in situ fracture toughness probe that allowed for measurement of a depth profile of fracture toughness in sediments in the field. Instead of using the geometry of a bubble extending a crack, a corkscrew-shaped probe was twisted in the sediment and pulled up, and fracture toughness calculated from the measured force using an equation for fracture of a screw that is pulled upward against a nut [17]. The tensile stress in the screw is amplified at the minor diameter between the threads of the screw, and when the stress amplification exceeds the fracture toughness of the material, a ring-shaped crack extends inward toward the center axis of the screw [25]. The probe tip is a helical coil that is screwed into the sediment such that the rotation rate (rev s^{-1}) exceeds the downward translation (mm s^{-1}) needed based on the coil spacing (rev mm^{-1}), resulting in a constant upward force [17] (Fig. 1A). This measured force is converted to fracture toughness using the equation derived by Oster and Mills [25] for fracture of a screw. This probe was used to measure fracture toughness profiles of muddy intertidal sediments at three sites in Nova Scotia, Canada [17] and in Willapa Bay, WA, USA [3].

2.2 Initial testing and modifications to fracture probe

The fracture probe [17] was designed for use in muddy sediments, and there were several considerations in using it in sandier, heterogeneous sediments and in clearly distinguishing whether fracture occurs. First, the probe needs to be robust enough to use in more granular sediments; and second, criteria for distinguishing whether fracture occurred or not need to be developed and tested.

First, preliminary testing of the probe designed by Johnson et al. [17] (Fig. 1A) was conducted in gelatin ($28.35 \text{ g (L seawater)}^{-1}$), a transparent analog for muddy sediments based on similar fracture behavior [18]. Gelatin in a glass aquarium was placed between crossed circular

polarizing filters to show stress fields, while the probe was used [12] (Fig. 1B). The first problem we observed was that the probe tip was not perfectly symmetrical, so rotation was not perfectly concentric, even in gelatin. The runout distance appeared to exceed the wire thickness and greatly expanded the initial crack length created by the wire. Stress fields around the wire grew and shrunk as it rotated, making the small wobble stand out visually. This difficulty in maintaining concentricity of the probe into a homogeneous material is likely to be amplified in heterogeneous sediments, in which large mineral grains or shell fragments could easily bend the wire out of alignment. Furthermore, deviations from concentric rotation would not be observable visually in opaque sediments, and we do not know how problems with alignment could otherwise be identified.

To identify the limit of cohesion of opaque muddy sediments, it was important to be able to clearly distinguish between fracturing and not fracturing from the probe data [17]. To visualize crack propagation, we rotated the probe 1 cm down into the gelatin, then stopped the rotation and pulled the probe upward all the way out of the gelatin. This should have driven a fracture across the inner diameter of the probe to break off an inner plug of gelatin. Instead, the crack propagated outward and extended to the surface to create a hole wider than the widest coil of the helix (Fig. 1C). Photoelastic stress analysis showed a considerable amount of stress outside of the coiled wire, rather than focused around the contact between the wire and the inner plug (Fig. 1B). For nut-loading fracture of a screw following the model of [25], tension applied should result in stress across the cross-sectional area that is amplified along the circumference of the screw. The connection to the surrounding gelatin allows the stress field to extend out from the coil, reducing the stress amplification at the inner part of the wire that should lead to fracture. To reproduce the stress distribution in a nut-loaded screw, the inner plug of sediment needs to be separated from the outer sediment. After some testing, the solution was to wrap the outer face of the coil in electrical tape, which is thin, has a low coefficient of friction, and was surprisingly robust to repeated use even in coarse sediments (Fig. 2B).

Given that the fracture probe [17] appeared to extend a fracture outward rather than inward from the coil, yet measured values of fracture toughness consistent with previous measurements, we examined the dependence of fracture toughness values on the geometry of the initial crack [27] (Supplementary material). Estimates of fracture toughness are somewhat robust to variation in the shape of the crack and the crack propagation direction (See Supplementary material for calculations). The closest analytical solution we could find to the probe when the outer sediment was not fully separated from the plug was a ring-

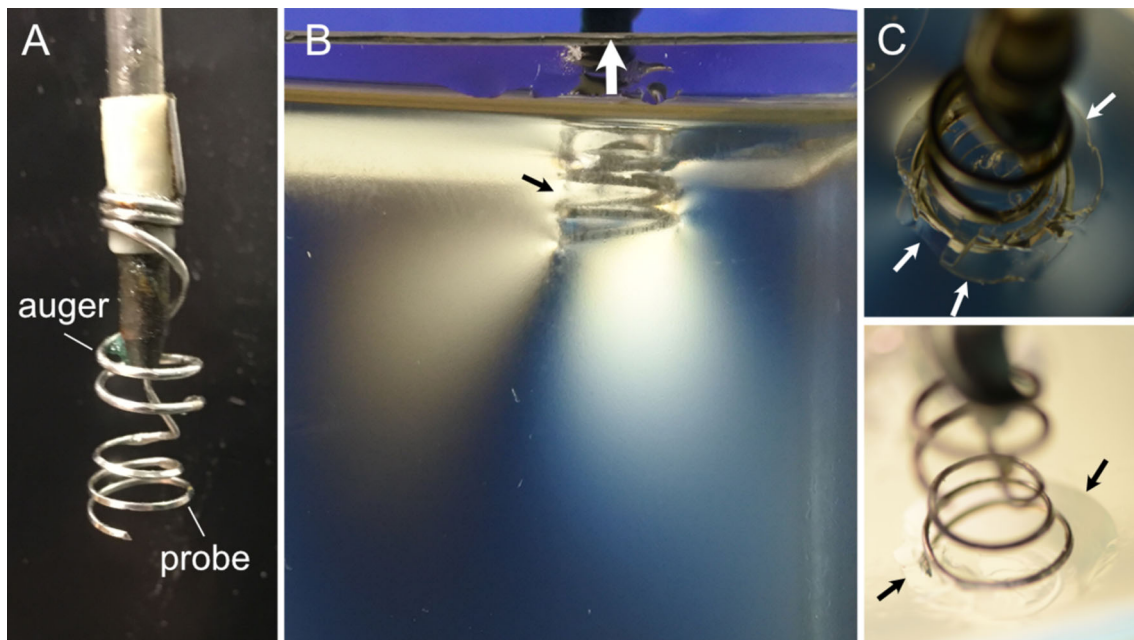


Fig. 1 **A** Tip of fracture probe developed by Johnson et al. [17], showing the helical probe with an auger above to clear sediment upward. **B** Image of the original probe in gelatin with stress shown as light regions through photoelastic stress analysis. The white arrow indicates the upward force applied to the probe. The stress field extends below the probe as the probe is pulled up as well as to the side through the gelatin connecting the inner part of the probe to the surrounding material (black arrow). **C** Top-down view of the probe after pulling up out of the gelatin (upper image) with polarizing filters in place and (lower image) from a more lateral view under natural light. Arrows indicate the edges of the hole

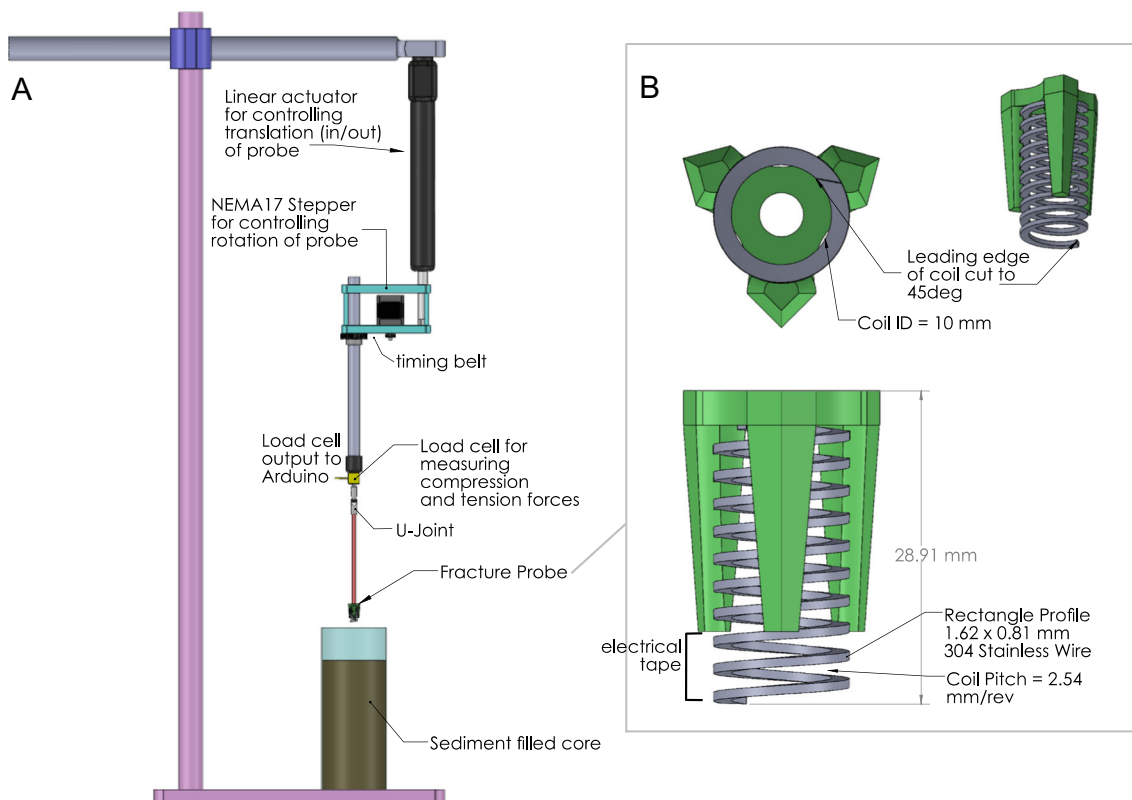


Fig. 2 **A** CAD drawing of probe instrument, with actuator for vertical translation, a stepper motor with gear for rotation, the inline 2 lbs load cell and thin rod holding the probe tip. **B** CAD drawing of probe tip from different angles

shaped crack, which our calculations indicate should propagate outward, consistent with our observations in gelatin, but with a fracture toughness relatively close to that predicted from the nut-driven screw model (Supplementary material). Previous measurements [17] may have underestimated fracture toughness by $\sim 28\%$.

The existing probe design continuously measures force as the probe is rotated into sediment, based on the assumption that by rotating the probe faster than it is translated downward, a constant tensile stress is applied. As the probe rotates, more stress is applied and the crack propagates, such that each force measurement corresponds with a critical amount of stress to extend the crack [17]. We separated rotation of the probe into the sediment from translation up to extend the crack by translating the probe upward at a velocity corresponding to the rotation rate (rev s^{-1}) divided by the coil spacing (rev mm^{-1}). This allowed for measurement of force as a function of distance. This force is expected to decrease when fracture occurs. Additionally, we found in early tests that the rotation of the probe caused noise in the force reading—this noise was considerably reduced when the probe was translating up or down with no rotation. This modification does reduce the vertical resolution of fracture measurements, as the probe needs to be rotated in enough to sufficiently grip the sediment before pulling up. Another issue with this larger displacement is that friction against the outer wall of the probe needs to be taken into account. We addressed this by repeating the cycle of rotation and translation to obtain a second force–distance profile. The force measured on the second pull includes friction with the sides and the weight of the sediment plug. This second force profile was subtracted from the first to obtain a net force representing the tensile strength or cohesion of the sediment.

2.3 Modified probe design

Our new probe tip is a coil with rectangular-profile wire (1.62×0.82 mm profile) with the wide side oriented horizontally allowing the narrow side to initiate the crack formation, following the theory from [25]. The fabrication of the coil was done on a metalworking lathe to ensure precision and repeatability of the operations. The rectangular-profile wire was captured in a custom-made holder that was mounted in the tool post of the lathe to maintain the desired profile orientation. The wire was then wrapped around a mandrel so that the resulting coil had an internal diameter of 10 mm and a coil pitch of 2.54 mm/revolution. The collet was machined on a CNC machine out of 6061 aluminum and consisted of 3 arms arranged equidistant around the outside of the wire coil. The internal faces of the collet arms had grooves machined into them, similar to a female thread, that matched the pitch of the wire coil. This

allowed the wire coil to be threaded into the collet body, which maintained the concentricity and pitch spacing of the coil as it was inserted into test substrates (Fig. 2B). The portion of the coil that extended past the collet arms was wrapped in electrical tape to separate the inner plug from the surrounding sediment (Fig. 2B) and the leading edge was angled at $\sim 45^\circ$.

The probe is translated up and down (X-direction) with a linear actuator (Ultra Motion Series U1 with a NEMA 17 stepper motor; Ultra Motion LLC, Cutchogue, NY) and rotated (Y-direction) clockwise (following the coil direction; Fig. 2B) with a stepper motor (NEMA 17, 0.9 deg/step) connected by a timing belt to the probe rod, with methods modified from Johnson et al. [17] (Fig. 2A). The motors are controlled with a TinyG v8 multi-axis motion controller (Synthetos.com) receiving serial G-code commands from an Arduino Zero microcontroller (12-bit Analog-to-digital converter). Tension and compression force data were generated from an in-line S-beam load cell (FUTEK LSB200, 2 lbs; FUTEK Advanced Sensor Technology, Inc., Irvine, CA) (Fig. 2A). Position and force data were read by the Arduino Zero and logged using an attached SD card shield and also displayed through the serial monitor in real time. Stop and resume buttons were included in the controller design to allow the user to quickly halt all movement to prevent damage to the probe or load cell if issues were encountered while in operation. The probe tip was mounted to a 20 cm long \times 6.35 mm diameter 316 stainless steel rod to prevent submersion of the load cell. The load cell was attached to the extension rod and probe with a U-joint to ensure vertical insertion of the probe. Wiring diagram and details on components and cost estimates are available (Supplementary Appendix 2).

Data were collected from 15 to 20 cm deep sediment cores at 10 mm depth increments starting at the surface of the core with a series of predefined movement commands referred to as a full cycle (Supplementary material, code 1). Before the first cycle begins, the probe tip is lowered to the sediment surface, which is set at $x = 0$ (Supplementary material, code 2). Each cycle consisted of two up-down movements: rotation at 0.23 revolutions s^{-1} while translating downward at 0.6 mm s^{-1} (the rotation rate multiplied by coil pitch of 2.54 mm/rev) for a distance of 10 mm; rotation stopped and translation upward at 1.67 mm s^{-1} for 10 mm (back to $x = 0$). This combination of rotation and translation results in no upward or downward force applied as the probe is screwed into the material. After two up-down movements at a depth, the probe rotates at 0.23 revolutions s^{-1} while translating downward at 0.6 mm s^{-1} for 10 mm to the next depth interval, and the position was zeroed to complete the cycle. One full cycle lasts ~ 1 min.

When fracture occurs, the force for the first cycle includes the force to break off the plug, to overcome friction with the sides, and to lift the weight of the plug of sediment. The force for the second cycle includes friction and sediment weight but not the force to overcome the tensile strength. Thus, a net force as a function of distance can be calculated by subtracting the second profile from the first. This net force profile is used to characterize cohesion and, when fracture occurs, fracture toughness is calculated from the peak net force.

3 Assessment

To ensure that the probe was effectively extending a crack inward from the coils, following the theory for fracture across the minimum diameter of a screw, we (1) tested the probe in gelatin to observe the stress distribution and ensure that stress amplification occurred in the inner ring of the coil. We then (2) used finite element modeling to predict the displacement needed for the stress intensity factor to exceed the fracture toughness and the crack to propagate inward, and (3) tested in sediments to ensure that the force data dropped at a displacement consistent with the model predictions and that a plug of sediment was broken off.

3.1 Testing in gelatin and sediment for effective fracture

We first tested the new probe in gelatin to ensure that the probe was operating as planned, however, we found that the probe consistently slipped out of the gelatin without breaking a plug, in contrast to tests in muddy sediments in which the probe consistently removed a plug of sediment. Force measurements from these gelatin tests showed no difference between the first and second upward displacement (Fig. 3A), and although a stress field was clearly visible below the probe, the probe appeared to have slipped upward (leaving a disturbed area in the gelatin below; Fig. 3B) and the forces measured were quite small. In contrast, tests in mud showed consistently higher first peaks, consistent with fracture (Fig. 3C). This was initially concerning, as we expected the probe to work effectively in both materials. We noted, however, that the distance that the probe was pulled upward before the peak force was on the order of several millimeters, much larger than the width of the wire (Fig. 3B,C). Force profiles from 1 cm depth in mud were similar to those in gelatin, showing overlapping force profiles and no net force (Fig. 3B). The probe frequently does not pull a plug at 1 cm depth in muds, whereas at deeper depths, there is a clear mud plug retained in the probe. We thus hypothesized that the friction

between the gelatin and the wire was insufficient to hold the gelatin for a large enough displacement to achieve fracture.

Although the probe did not successfully fracture the gelatin, the videos and force profiles provide important insight into the functioning of the probe. First, we observed some stress around the sides of the probe (Fig. 3B), but this stress field did not appear visually different before and after the probe pulled up. Stress fields were likely due to the probe pushing against the outer walls of the hole and preventing collapse of the gelatin. We also tested the probe in muddy sediment with and without the electrical tape to separate the plug from the surrounding sediment. Peak forces were considerably higher without the electrical tape, resulting in greater estimated fracture toughness (Fig. 3D). Thus, the tape seems to be effective at separating the plug from the surrounding sediment, and fracture likely occurs inward across the bottom of the plug. Second, we also observed a change in the stress field below the plug as the actuator moved up, with stress decreasing over a short distance then increased again. We interpreted this as compressive stress from the insertion of the probe, corresponding to the minima in force before the start of the upward pull (Fig. 3A). Compressive stress is released as the probe moves up, then tensile stress increases (Fig. 3B). This is consistent with observations of residual strain in gels resulting from needle insertion [2] and with low force at the beginning of the upward pull in sediment (Fig. 3C).

3.2 Finite element modeling of fracture probe

Our data suggesting that the probe needed to be pulled up several mm before fracture would occur was initially surprising, as the original probe design did not incorporate this much displacement [17]. To determine if this estimate was consistent with mechanics and to better understand how that distance depends on the material properties of the sediment or gelatin, we developed a simplified model of the probe using the finite element modeling program, Abaqus (Simulia, Dassault Systemes).

To calculate the stress intensity factor at the crack tip resulting from upward displacement of the probe, we developed a simplified 2-D axisymmetric model of the probe using Abaqus/CAE software with a crack tip defined following theory (Fig. 4A). The probe was modeled as an outer ring of 0.5 mm thickness (an overestimate of the electrical tape thickness) encircling a plug of 6.12 mm radius (outer radius of the probe), a simplification of the more complex 3-D geometry. At the bottom of the ring is a wire that extends 1.64 mm toward the center of the probe, leaving an inner plug diameter of 9.96 mm (Fig. 4A). This surface represents the bottom coil of the probe. The probe is positioned at 30 mm depth in a 15 cm diameter, 15-cm

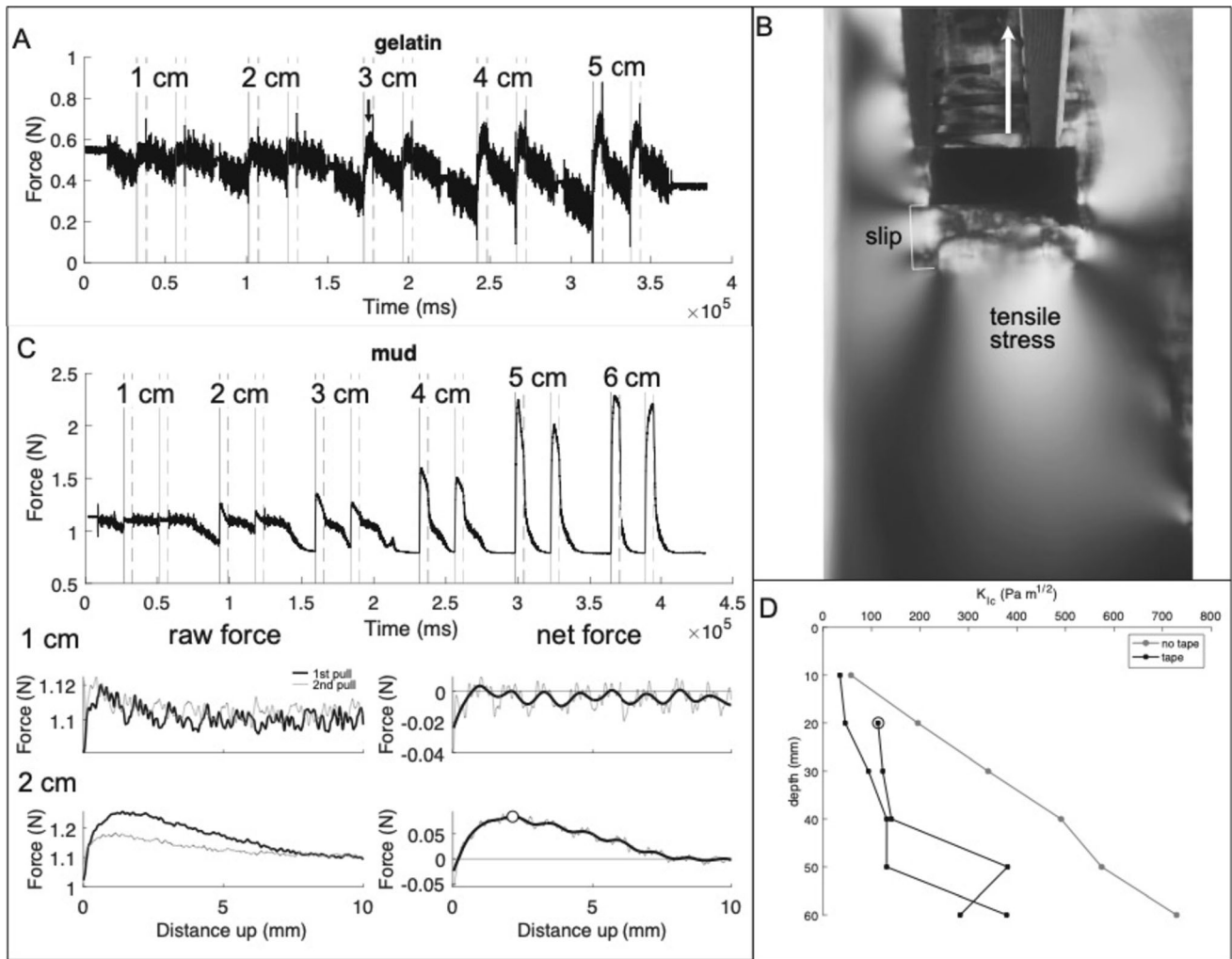


Fig. 3 **A** Raw data of force profile in gelatin at 1 cm intervals to 5 cm depth. Vertical lines show beginning (solid) and end (dashed) of two upward pulls at each depth. There was no difference in force between subsequent upward pulls at any depth. **B** Image of probe at 3 cm depth in gelatin using photoelastic stress analysis, taken at the peak of the upward pull indicated by the black vertical arrow in (A), showing upward slipping of the probe at peak force. **C** Raw data of force profile in muddy sediments at 1 cm intervals to 6 cm depth, showing first peak higher than 2nd for all depths below 1 cm. Raw force over the 1 cm upward pull at 1 and 2 cm depths is shown below on the left, with net force (first pull–second pull) on the right. **D** Fracture toughness depth profiles in mud with tape (black) and without tape (gray). Black circle indicates the fracture toughness corresponding to the peak force at 2 cm for the profile shown in (C)

deep container with fixed outer sides and bottom. The probe is tied to the sediment on the inner edge (tie constraint with nodes matching between the probe and sediment parts) and is allowed to slip with no friction along the outer edge. Fracture modeling in Abaqus requires the position and direction of the crack to be pre-defined; therefore, a crack tip is defined at the inner tip of the probe and the direction of crack propagation inward toward the plane of symmetry was varied to determine the most likely direction of crack propagation. An upward displacement is applied to the top surface of the probe, mimicking the actuator motion. The sediment was meshed with quadratic quadrilateral elements, type CAX8R.

First, the model was run with gelatin as the material (stiffness: $E = 1900$ Pa, Poisson's ratio: $\nu = 0.45$, density: $\rho = 1035$ kg m⁻³) to determine the displacement distance required to cause a stress amplification sufficient to exceed the fracture toughness. The direction of crack propagation was determined by running the model with different crack propagation directions to find the direction at which K_I was highest and K_{II} (the out of plane stress amplification) was close to 0, $\sim 34^\circ$ above horizontal. Then, displacement was increased incrementally until K_I reached K_{Ic} of 58.1 Pa m^{0.5} for gelatin [11]. Since this was a linear model, both the force associated with the displacement and the resulting stress intensity factor scaled linearly with the displacement. K_I reached K_{Ic} at 3.2 mm displacement, resulting in a force

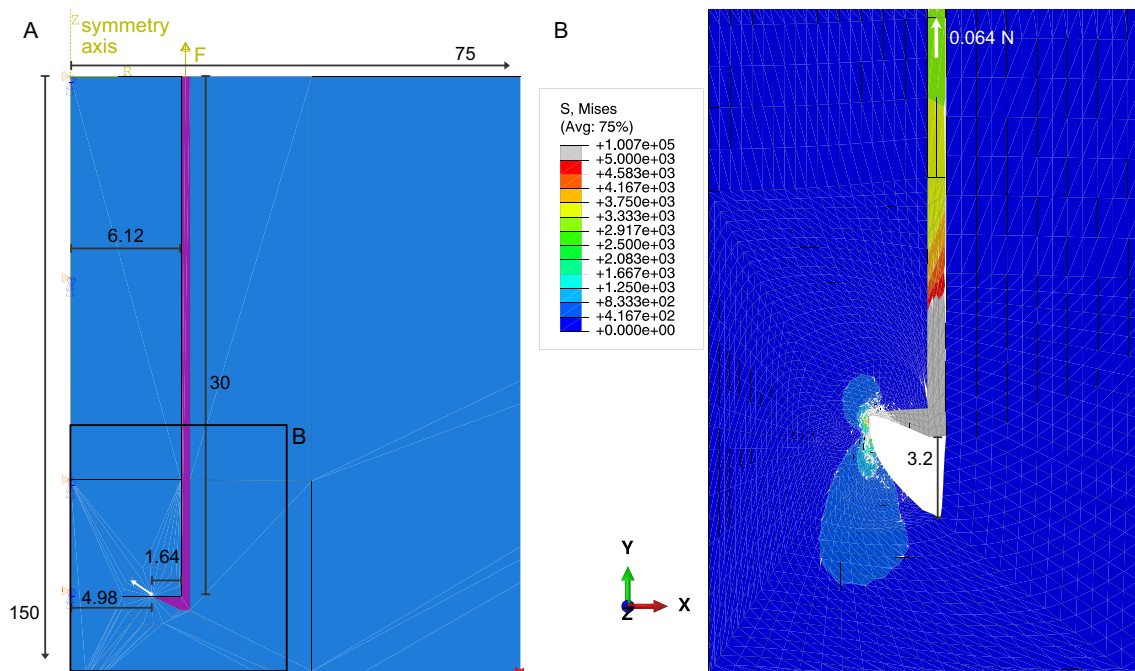


Fig. 4 **A** 2-D axisymmetric model of probe, showing probe in magenta, gelatin in blue, and direction of crack propagation as white arrow. The left border is the axis of symmetry, and the model extends radially and downwardly beyond the field of view. **B** Deformed mesh around the probe (region indicated with black box in **A**) when the probe displacement results in a K_I at the crack tip that reaches K_{Ic} for gelatin. The force (N) resulting from the applied displacement is given at the top. All other numbers are dimensions in mm. Color bar shows von Mises stresses in the material

of 0.064 N (Fig. 4B). Changing the stiffness of the model to muddy sediment ($E = 27$ kPa) instead of gelatin [10] confirmed that the displacement needed to achieve fracture increases linearly with fracture toughness and decreases with stiffness. Thus, the displacement is directly proportional to the ratio of fracture toughness to stiffness, as expected from the linear model. Gelatin and sediment have comparable K_{Ic}/E , but gelatin is slightly tougher [18], indicating that the probe displacement should be slightly smaller in sediment, although natural sediments vary considerably in both K_{Ic} and E .

It is important to note that this 2-D model (Fig. 4) only roughly approximates the probe geometry and assumes linear elastic deformation and fracture. These assumptions are appropriate for gelatin, although the exact value of displacement should be interpreted with some caution, but there are some considerations in extrapolating these results to sediments. The model does not consider effective stress in natural sediments; this stress from overlying sediment may increase the force needed for fracture in sediments. It is likely that the friction coefficient between sediment and the probe is greater than that between gelatin and the probe due to the grains in sediment, allowing for the probe to pull up further without slipping. However, sediment can also yield when the stress in the material (color bar; Fig. 4B) exceeds the strength. Thus, when K_{Ic}/E is high, the probe is likely to fail either by slipping or through yielding of the

sediment. The highest stress occurs below the tip of the probe (Fig. 4B), where the material is stretched as the probe is pulled up. This suggests that if failure occurs through yielding, that the direction of the failure plane will be oriented downward, resulting in a convex plug, in contrast to the upward oriented crack propagation direction, which would result in a concave plug.

3.3 Evaluation of probe data along sediment gradients

The probe was tested iteratively throughout development in sediments collected from around coastal Alabama. Data shown here are from 10 cm diam cores collected by AAUS divers from sediments offshore of Dauphin Island and Ft. Morgan peninsula in September 2020 and were selected as representative cores that illustrated the different sediment responses observed. The examples shown here were collected from a site 20 m deep offshore of Dauphin Island (T1 20 m, 30° 6.255' N, 88° 0.415' W) before (Fig. 5A) and after (Fig. 5B) Hurricane Sally passed over the area, depositing sand at this site [7]. Storm disturbance likely also caused vertical layering observed in sediments at other sites that were clearly distinguished from grain size data and the probe measurements of tensile strength (Fig. 5C, D). Example data shown are from two 12-m deep sites, T3 12 m (30° 12.736' N, 88° 13.072' W) and T4 12 m (30°

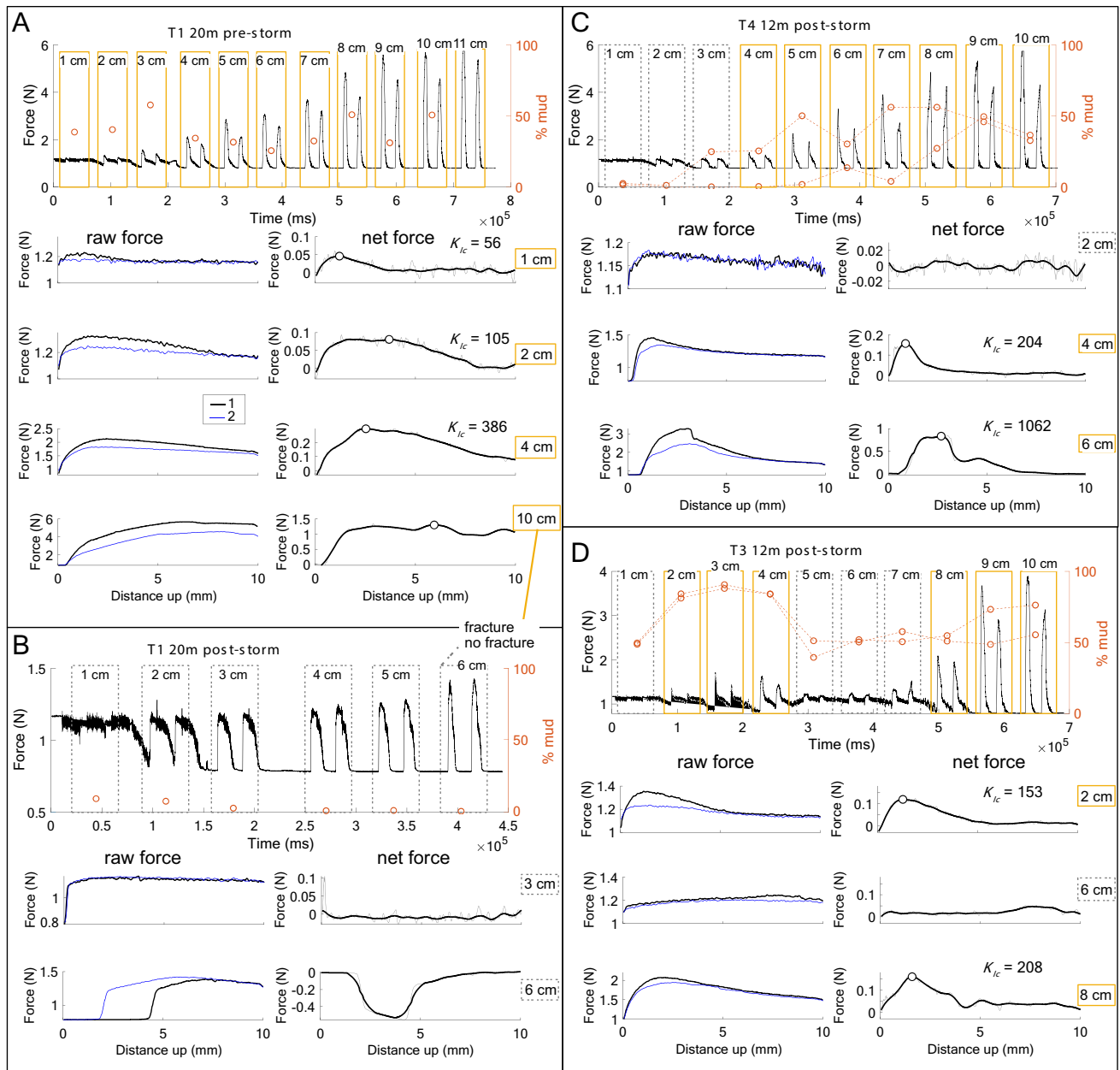


Fig. 5 Force data from fracture probe profiles in 4 sediment cores collected at 12 or 20 m depths offshore of Dauphin Island, AL, shortly before (Sept. 10–11, 2020; pre-storm) or after (Sept. 26–27, 2020; post-storm) Hurricane Sally passed over the study area. **A** Muddy sediments at 20 m depth before the storm, **B** Sediment core from the same site as A after the storm passed and deposited a thick layer (> 6 cm) of sand. **C** Post-storm site (12 m depth) showing a layer of sand on top of mud. **D** Post-storm site (12 m depth) showing vertical layering. Upper plots show raw force profiles over time as the probe was rotated into then translated up out of sediments twice at each 1-cm depth interval. Vertical lines show the beginning (solid) and end (dashed) of the upward pull, with the first pull in black and second in blue. Percent mud content (< 0.063 mm) is plotted for each depth as a red ‘o,’ with duplicate cores plotted separately. Shown below is raw force as a function of vertical position on the left (first pull in thicker black line, second in thinner blue line) and net force on the right (raw data in thin gray line, smoothed data in thicker black line, with black ‘o’ at peak force) for selected depth intervals. Orange solid boxes indicate measurements in which sediments were cohesive; gray dashed boxes indicate measurements in which no fracture occurred. Calculated K_{Ic} is given in $\text{Pa m}^{0.5}$

11.690' N, 88° 4.950' W), off the west end of Dauphin Island and south of Ft. Morgan, respectively.

In the muddier pre-storm example core (with ~ 30–60% mud, < 0.063 mm), and other cores from cohesive muddy sediments (data not shown), the first peak

is consistently higher than the second peak, resulting in a positive net force corresponding to fracture toughness (Fig. 5A). With increasing depth in the sediment, the peak becomes broader with a less pronounced drop in force corresponding to fracture (Fig. 5A). In sandier cores such

as the post-storm example core (< 10% mud), the force peaks are smaller, and there is no difference between the first and second force profiles (Fig. 5B). Post-storm cores from other sites showed vertical layers, e.g., non-cohesive sandier sediment that did not fracture on top of muddier sediment that did fracture (Fig. 5C) or more complex vertical layering (Fig. 5D). Interestingly, sandy mud layers (~ 40–60% fines) clearly fractured in some cores (Fig. 5A, C) but showed no tensile strength in others (Fig. 5D). Although the distinction between cohesive and non-cohesive behavior is often clear from the raw force data as a higher force in the first pull (upper graphs, Fig. 5A, B), raw force–distance curves and net force–distance curves provide important detail when peaks are small (e.g., Fig. 5A, 1 cm; C, 4 cm; D, 2, 6 cm). Sediments were characterized as non-cohesive, or lacking tensile strength, when raw force profiles as a function of distance overlap, and net force is close to 0 with no clear peak (e.g., Fig. 5B, 3 cm; 2 cm; D, 6 cm). In some cases, the net force is small but positive (Fig. 5D), and the presence or absence of a peak is important in distinguishing cohesive from non-cohesive behavior. Forces are often very small at 1 cm depth (Fig. 5), and while a net force peak can sometimes be distinguished (Fig. 5A), the lack of a clear peak at this depth can be difficult to interpret. The probe likely slips due to low stiffness or low yield strength of surface sediments (Figs. 3, 4). Note that force peaks at a distance of ~ 2–3 mm, consistent with the finite element modeling results (Fig. 4B), and calculated fracture toughness, K_{Ic} , falls close to or within the expected range of ~ 280–550 Pa m^{-0.5} [18] (Fig. 5).

Some issues with probe functioning can be observed at greater depths in both muddy and sandy cores. Deeper in muddy cores, raw force often does not drop off during the first pull, instead increasing to an asymptote for both profiles (Fig. 5A, 10 cm). The force is consistently higher for the first pull, but net force does not drop to 0, indicating the plug may not have broken off completely, and the peak in net force can be difficult to distinguish. Because the net force is positive, we consider this response cohesive, but the broader peak indicates more ductile fracture, which is inconsistent with previous measurements of fracture toughness using bubble injection in which bubble growth was well predicted by linear elastic fracture mechanics, indicating brittle fracture [18]. The maximum limit of the load cell is also occasionally reached in muds (Fig. 5A, 11 cm; C, 10 cm). This could be resolved with a larger load cell, but the force data generally become difficult to interpret before the force maxes out. In sands, the compressive force as the probe is rotated into the sediment increases with depth, e.g., reaching the minimum load cell reading by 3 cm depth in Fig. 5B. While this compressive force does not immediately affect the raw force, by 6 cm

depth in this core, the probe is pulled up almost 5 mm before the compressive force is reduced and tensile force starts to increase (Fig. 5B). The resistance to probe penetration appears to be reduced by the first insertion because the force increases at a lower depth (smaller distance) on the second pull, resulting in a misalignment of the force profiles and an apparent negative net force (Fig. 5B). This appears to be a limitation in the design of the probe; increasing the distance between threads or using a thinner wire (Fig. 2B) may reduce the resistance to penetration but would also decrease the vertical resolution of measurements and the robustness of the probe.

4 Discussion and future directions

The probe shows clearly distinct responses in muddier versus sandier sediments, with a higher force peak for the first upward pull in cohesive sediments but no difference in force between the two subsequent pulls in non-cohesive sediments. In addition, we identified and resolved several issues in measuring fracture toughness using this method [17]. Although the probe seems to effectively distinguish cohesive from non-cohesive sediments and to measure fracture toughness of muddy sediments, the depth range is somewhat limited.

Near the surface (1–2 cm), force measurements are very low, often not detectable above the noise. This is consistent with the probe not holding and breaking off a plug: either the probe slips or the sediment yields rather than fracturing. This could result from the material properties of the mud: if the stiffness is low relative to toughness, the probe may slip, or if the yield strength is low, the sediment may fail before enough force can be applied to reach the fracture toughness. Surface sediments are less consolidated [31], and yielding of high-porosity sediments is not surprising. This may, however, be an artifact from the design of the probe. The initial penetration of the probe into sediment is not always straight, because the long rod is allowed to rotate around the U-joint. Within a few mm, it straightens out, but the upper layer of sediment is disrupted. This is unfortunate, as erosion experiments suggest that there may be interesting transitions in sediment cohesion within this surface layer [29]. Additionally, observations of worms burrowing down into sediments suggest that there may be some transition in failure mechanisms at ~ 1–2 cm. The polychaete, *Alitta virens*, initially crawls along the sediment surface and then burrows down into the sediment at a shallow angle. As it burrows, the gait transitions from steady crawling to more punctuated movements, in which the tail pulls forward then the body pauses (Dorgan, unpublished data). This behavior is consistent with transitioning from burrow extension by pushing the sediment

grains aside to incremental burrow extension by fracture. Further work to better measure cohesion in the surface 1–2 cm layer could provide important insight to both burrowing mechanics and behaviors and subsurface erosion.

As the probe goes deeper (> 5–6 cm), the peak in force becomes flatter and the force no longer drops to 0 within the 1 cm upward pull of the probe. The net force peak becomes more difficult to distinguish, raising questions about the accuracy of calculated fracture toughness. In addition, calculated fracture toughness increases substantially with depth (Fig. 5). This is consistent with a transition from brittle to ductile fracture observed in rocks under increasing confining pressure [16]. Ductile fracture at 7–10 cm depth in muds is surprising, however, as it contrasts with findings of bubble growth by linear elastic fracture mechanics at ~ 20 cm depth in sediments [18]. A key difference between the fracture toughness probe and bubble injection is that air is injected during bubble injection. It is possible that the air injection partially compensates for the increasing confining pressure from the weight of the overlying sediment with depth. Further work to compare fracture toughness measurements from this fracture probe with those from bubble injection is needed to better understand this apparently ductile behavior. The impacts of infauna are primarily in the top 6–10 cm, corresponding to the mean mixed layer depth for bioturbation [4, 28]. Deeper measurements could potentially show a transition in tensile strength at the bottom of the mixed layer and allow for geotechnical measurement of the mixed layer depth.

Although the depth range is limited, the ability to distinguish sediments that exhibit tensile strength from non-cohesive, granular sediment behavior has important implications in understanding how sediment properties such as grain size, porosity, and organic content contribute to tensile strength, as well as the spatial and temporal variability in cohesion in dynamic coastal systems. This distinction also has implications for characterizing habitats for infaunal communities and predicting sediment stability. Cohesive and non-cohesive sediments differ in their erodibility in response to surface shear stress [31]. Cohesion can result from EPS secreted by microalgae and microbes [6] as well as from electrochemical attraction between clay particles. This novel sub-surface measurement allows for relating surface properties measured through erodibility (e.g., with a Gust chamber, [29]) to subsurface tensile strength. This is relevant, e.g., when a microalgal mat stabilizes surface sediments but may not penetrate very deep.

Supplementary Information The online version contains supplementary material available at <https://doi.org/10.1007/s11440-023-02134-6>.

Acknowledgements We thank Bruce Johnson, Mark Barry, and Bernie Boudreau for their previous work on developing this instrument and for their advice and expertise. We also thank Sanjay Arwade for help with the finite element modeling.

Funding This work was funded by the Office of Naval Research Awards N00014-17-1-2625, N00014-18-1-2806, N00014-20-1-2377, and N00014-21-1-2214 to KMD. GL was supported through base funding from the Office of Naval Research to the US Naval Research Lab.

Open Access This article is licensed under a Creative Commons Attribution 4.0 International License, which permits use, sharing, adaptation, distribution and reproduction in any medium or format, as long as you give appropriate credit to the original author(s) and the source, provide a link to the Creative Commons licence, and indicate if changes were made. The images or other third party material in this article are included in the article's Creative Commons licence, unless indicated otherwise in a credit line to the material. If material is not included in the article's Creative Commons licence and your intended use is not permitted by statutory regulation or exceeds the permitted use, you will need to obtain permission directly from the copyright holder. To view a copy of this licence, visit <http://creativecommons.org/licenses/by/4.0/>.

Data availability The datasets generated during and analyzed during the study are available from the corresponding author upon reasonable request.

References

- Anderson TL (2005) Fracture mechanics, 3rd edn. CRC Press, Boca Raton
- Barney CW, Zheng Y, Wu S, Cai S, Crosby AJ (2019) Residual strain effects in needle-induced cavitation. *Soft Matter* 15:7390–7397. <https://doi.org/10.1039/c9sm01173k>
- Barry MA, Johnson BD, Boudreau BP, Law BA, Page VS, Hill PS, Wheatcroft RA (2013) Sedimentary and geo-mechanical properties of Willapa Bay tidal flats. *Cont Shelf Res* 60S:S198–S207. <https://doi.org/10.1016/j.csr.2012.05.007>
- Boudreau BP (1998) Mean mixed depth of sediments: the wherefore and the why. *Limnol Oceanogr* 43:524–526
- Boudreau BP, Algar C, Johnson BD, Croudace I, Reed A, Furukawa Y, Dorgan KM, Jumars PA, Grader AS, Gardiner BS (2005) Bubble growth and rise in soft sediments. *Geology* 33:517–520. <https://doi.org/10.1130/g21259.1>
- Chen XD, Zhang CK, Zhou Z, Gong Z, Zhou JJ, Tao JF, Paterson DM, Feng Q (2017) Stabilizing effects of bacterial biofilms: EPS penetration and redistribution of bed stability down the sediment profile. *J Geophys Res Biogeosci* 122:3113–3125. <https://doi.org/10.1002/2017jg004050>
- Clemo W, Dorgan K, Wallace D, Dzwonkowski B (2023) Effects of Hurricane Sally (2020) on sediment structure and infaunal communities in coastal Alabama. *Proc Coast Sediments* 2023:1055–1068
- de Brouwer J, Wolfstein K, Ruddy GK, Jones TER, Stal LJ (2005) Biogenic stabilization of intertidal sediments: the importance of extracellular polymeric substances produced by benthic diatoms. *Microb Ecol* 49:501–512. <https://doi.org/10.1007/s00248-004-0020-z>

9. Dorgan KM (2015) The biomechanics of burrowing and boring. *J Exp Biol* 218:176–183. <https://doi.org/10.1242/jeb.086983>
10. Dorgan KM, Arwade S, Jumars PA (2007) Burrowing in marine muds by crack propagation: kinematics and forces. *J Exp Biol* 210:4198–4212
11. Dorgan KM, Arwade S, Jumars PA (2008) Worms as wedges: effects of sediment mechanics on burrowing behavior. *J Mar Res* 66:219–254
12. Dorgan KM, Jumars PA, Johnson BD, Boudreau B, Landis E (2005) Burrow extension by crack propagation. *Nature* 433:425. <https://doi.org/10.1038/433475a>
13. Dorgan KM, Jumars PA, Johnson BD, Boudreau BP (2006) Macrofaunal burrowing: the medium is the message. *Oceanogr Mar Biol* 44:85–121
14. Gardiner BS, Boudreau BP, Johnson BD (2003) Growth of disk-shaped bubbles in sediments. *Geochim Cosmochim Acta* 67:1485–1494
15. Grabowski RC, Droppo IG, Wharton G (2011) Erodibility of cohesive sediment: the importance of sediment properties. *Earth-Sci Rev* 105(3–4):101–120
16. Hu K, Zhu Q, Chen L, Shao J, Liu J (2018) A micromechanics-based elastoplastic damage model for rocks with a brittle-ductile transition in mechanical response. *Rock Mech Rock Eng* 51:1729–1737. <https://doi.org/10.1007/s00603-018-1427-z>
17. Johnson BD, Barry MA, Boudreau BP, Jumars PA, Dorgan KM (2012) In situ tensile fracture toughness of surficial cohesive marine sediments. *Geo-Mar Lett* 32:39–48. <https://doi.org/10.1007/s00367-011-0243-1>
18. Johnson BD, Boudreau BP, Gardiner BS, Maass R (2002) Mechanical response of sediments to bubble growth. *Mar Geol* 187:347–363
19. Jumars PA, Nowell ARM (1984) Effects of benthos on sediment transport: difficulties with functional grouping. *Cont Shelf Res* 3:115–130
20. Mayer LM (1994) Surface area control of organic carbon accumulation in continental shelf sediments. *Geochim Cosmochim Acta* 58:1271–1284
21. Meadows PS, Tait J (1989) Modification of sediment permeability and shear strength by two burrowing invertebrates. *Mar Biol* 101:75–82. <https://doi.org/10.1007/bf00393480>
22. Meysman FJR, Middelburg JJ, Heip CHR (2006) Bioturbation: a fresh look at Darwin's last idea. *Trends Ecol Evolut* 21:688–695. <https://doi.org/10.1016/j.tree.2006.08.002>
23. Mitchell J, Soga K (2005) *Fundamentals of Soil Behavior*, 3rd edn. Wiley, Hoboken
24. Murray JMH, Meadows A, Meadows PS (2002) Biogeomorphological implications of microscale interactions between sediment geotechnics and marine benthos: a review. *Geomorphology* 47:15–30
25. Oster DM, Mills WJ (2000) Stress intensity factor solutions for cracks in threaded fasteners. In: Toor P (ed) *Structural integrity of fasteners: second volume*, ASTM STP 1391: 85–101
26. Rhoads DC, Stanley DJ (1965) Biogenic graded bedding. *J Sediment Res* 35:956–963. <https://doi.org/10.1306/74d713bb-2b21-11d7-8648000102c1865d>
27. Sih GC (1973) *Handbook of stress-intensity factors*. Lehigh University, Bethlehem
28. Teal LR, Bulling MT, Parker ER, Solan M (2008) Global patterns of bioturbation intensity and mixed depth of marine soft sediments. *Aquat Biol* 2:207–218. <https://doi.org/10.3354/ab00052>
29. Thomsen L, Gust G (2000) Sediment erosion thresholds and characteristics of resuspended aggregates on the western European continental margin. *Deep Sea Res Part Oceanogr Res Pap* 47:1881–1897. [https://doi.org/10.1016/s0967-0637\(00\)00003-0](https://doi.org/10.1016/s0967-0637(00)00003-0)
30. Volkenborn N, Polerecky L, Wetthey DS, Woodin SA (2010) Oscillatory porewater bioadvection in marine sediments induced by hydraulic activities of *Arenicola marina*. *Limnol Oceanogr* 55:1231–1247. <https://doi.org/10.4319/lo.2010.55.3.1231>
31. Wheatcroft RA, Wiberg PL, Alexander CR, Bentley SJ, Drake DE, Harris CK, Ogston AS (2007) Postdepositional alteration and preservation of sedimentary strata. In: *Continental margin sedimentation*. pp 101–155

Publisher's Note Springer Nature remains neutral with regard to jurisdictional claims in published maps and institutional affiliations.